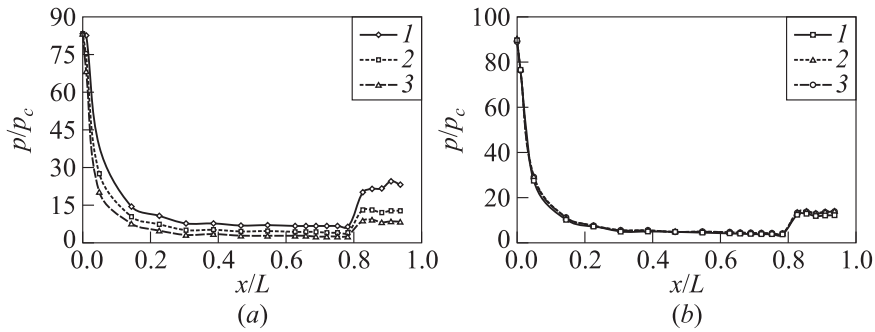

Figure 14 Pressure distribution at M = 7.8 at $\alpha = 0°$ (a) and $\alpha = 6°$ (b): *1* — $\gamma - 0°$; *2* — 90°; and *3* — $\gamma = 180°$

to possible separation of the boundary layer due to its interaction with the shock wave. Subsequent Navier–Stokes calculations confirmed the presence of the separation zone in the flap region. Note also that the pressure distributions outside the separation region almost coincide in viscous and inviscid calculations.

The foregoing results on the pressure distribution are related to the EXPERT 4.2 modifications. The data for EXPERT 4.4 modifications were also obtained at M = 7.8 (Fig. 14). Figure 14*a* shows the dependencies of relative pressures $p/p_\infty = f(x/L)$ measured at the zero angle of attack for the rolling angles $\gamma = 0°$ and 180°. The obtained results indicate the symmetrical flow around the model, absence of flow angularities, and satisfactory degree of the velocity field nonuniformity in the test section. Figure 14*b* presents similar pressure distributions for the angle of attack $\alpha = 6°$, measured in different planes of symmetry ($\gamma = 0°$ — windward side, $\gamma = 90°$ — side surface, and $\gamma = 180°$ — leeward side). In dependence of the rolling angle, all three pressure distributions are divided into layers and the boundary-layer separation ahead of the flap with consequent reattachment is observed.

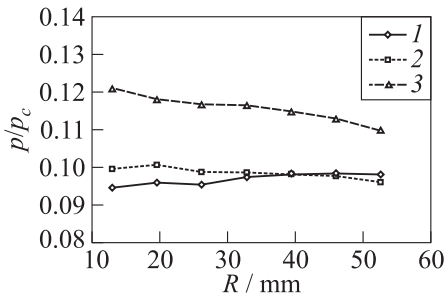

Figure 15 Distribution of base pressure at M = 7.8: *1* — $\theta = 0°$; *2* — 90°; and *3* — $\theta = 180°$

The relative pressure distribution on the base section of the model at the angle of attack $\alpha = 6°$ is given in Fig. 15 where R is the distance from the axis of the base section to the measurement point. It is clearly seen that the radial pressure distribution at $\theta = 0°$ (windward surface) and $\theta = 90°$

(horizontal symmetry plane) lie in the confidential interval of the error. As for the differences of the pressure distribution on the base section (leeward surface region $\theta = 180°$), it should be noted that the values correspond to the measurement points positions in the vertical plane of the model symmetry for the angle of attack 6°. It should also be mentioned that the absolute values of the pressure on the EXPERT-model base surface are very small and reach $\sim$ 10%–12% from the static pressure in the free stream.

6 DISTRIBUTION OF HEAT FLUXES ON THE SURFACE

Heat fluxes were investigated in the wind tunnel AT-303 at M = 13.93, $\alpha = 0°$, $\mathrm{Re}_1 = (2.36\text{–}2.43) \cdot 10^7$, $T_0 = (1260\text{–}1300)$ K, $P_0 \approx 108$ MPa for the EXPERT 4.4 model version. The period of the flow working mode existence was about 70 ms. The model was made of Plexiglas (scale 1:8) and had replaceable nose units permitting to form steps in the section of the nose part and body junction. The step was 1 mm for the model 2 and 2 mm for the model 3. Thermal loads were measured by two methods: (*i*) the discrete method involving calorimetric gages of heat fluxes, and (*ii*) the panoramic infrared (IR) method based on IR thermography (IRT). The calorimetric gages were installed on two model generatrics: in the flap plane of symmetry ($\theta = 0°$, 20 gages) and in the plane between the flaps ($\theta = 45°$, 5 gages). The error of the heat flux measurement did not exceed 10% from the measured value.

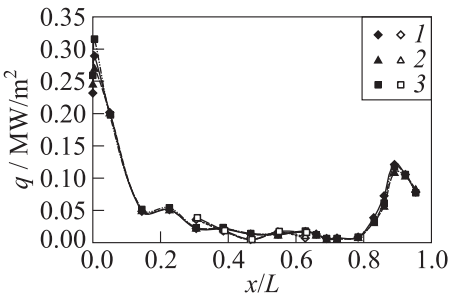

Figure 16 Heat fluxes distribution over the surface of the model without step for different runs: *1* — 2405; *2* — 2406; and *3* — 2408. Empty signs refer to conical nozzle

Heat fluxes distribution toward model 1 obtained with the aid of calorimetric gages (Fig. 16) shows that the maximum level of the specific heat flux, which is about 0.3 MW/m^2, was reached on the nose part surface, somehow downstream from the stagnation point. Before the flap, the flow separates and then reattaches on the flap surface. The separation region length, found from the minimum level of the heat flux 0.005–0.007 MW/m^2, is about 20–25 mm. In the flow reattachment region (approximately on the flap center), the heat flux level has the maximum, and then it decreases in the tail part. The value of the maximum heat flux on the flap surface, according to the results of multifold measurements, varied from 0.12 to

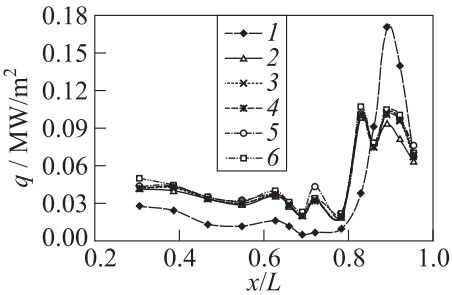

Figure 17 The influence of the surface roughness on heat fluxes to the surface for different runs: *1* — 2435; *2* — 2436; *3* — 2437; *4* — 2438; *5* — 2439; and *6* — 2440

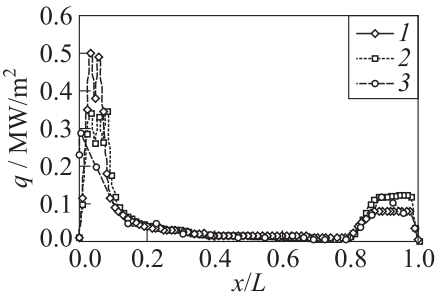

Figure 18 Comparison of heat fluxes distributions obtained by calorimetric (*1* — 30 ms; and *2* — 40 ms) and IR gages (*3*)

0.17 MW/m^2, which may result from the nonstationary flow in the reattachment region. On the flat unit of the model surface before the flap, practically constant heat-flux level is kept up to the separation region. At the same time, on the cone surface, the heat-flux level near the nose part is two times higher than on the flat section, and decreases essentially downstream.

To study the influence of the flow turbulization in the boundary layer, model 2 was tested with the increased surface roughness, which was provided by the powder of about 200 μm sprayed on the nose part surface. The results of heat fluxes measured by the calorimetric method are shown in Fig. 17 in comparison with the initial version (without turbulization). Increased relative surface roughness in the model nose part resulted in the essential increase of the heat flux levels over the body, decrease of the separation region length before the flap, and thermal load redistribution over the flap surface, the maximum heat flux level being decreased. These results can apparently be caused by the changing character of the flow in the boundary layer, which was, due to the increased roughness of the nose part, transformed from the laminar to turbulent mode.

Figure 18 shows the comparison of the heat fluxes measured by the calorimetric and thermography methods. Good agreement between the data obtained on the model body surface within the working mode time of about 30–40 ms is observed. Somehow bigger scatter in the data on the nose part can result from the registered overtemperatures against the rated temperature range of the IR camera and essentially changing foreshortening.

Data scattering on the flap is apparently caused by the flow nonstationary in the reattachment region.

The panoramic method of measurements with high spatial resolution permitted (in contrast to the discrete method) to define the size of the separation

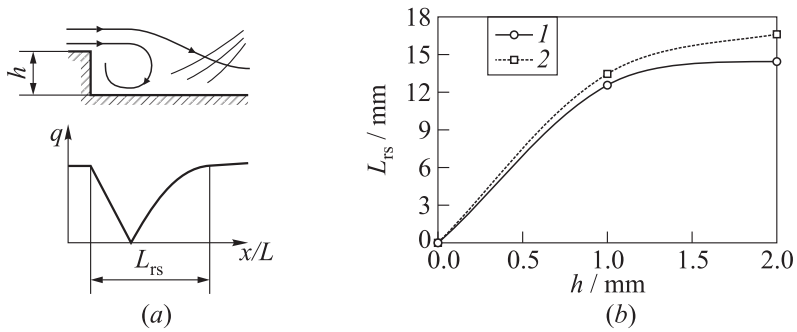

Figure 19 The influence of the step height on the separation region size: *1* — $\gamma = 0°$; and *2* — $\gamma = 45°$

regions formed before the flaps and in the area of the nose part and body. In particular, it was shown that the separation region resulted from the interaction between the shock wave generated by the flap and the boundary layer on the body exceeds the side bounds of the flap. The length of the separation region has its maximum in the flap plane of symmetry and decreases when moving off from this plane. The maximum size of the separation region (21–23 mm) is in good agreement with the calorimetric measurements data. Maximum temperature levels realize near the flap leading edge and side edges.

In the point of nose part and body junction, with the step being present (models 2 and 3), the separation region formation downstream is followed by the flow reattachment. The separation region length increases essentially when the step height rises, as is shown in Fig. 19 for the flat ($\theta = 0°$) and conic ($\theta = 45°$) sections of the body surface. The separation region length is somehow bigger on the conic surface ($\theta = 45°$) than on the flat section ($\theta = 0°$).

We do not observe any essential growth of the thermal load level (in respect to model 1) in the region of reattachment of the flow separated because of the step. Thermal load redistributions (in respect to model 1), observed in the area of the studied sizes of the step, do not cause any considerable influence on the separation region forming before the flap.

7 CONCLUDING REMARKS

Investigations of the total aerodynamic characteristics of the EXPERT 4.2 model performed in hypersonic wind tunnels T-313 and AT-303 ITAM SB RAS with the countered nozzle within the Mach numbers range M = 4–14 show the following:

– the longitudinal force coefficient weakly depends on the angle of attack within the range of α from -3° to 6° for any free-stream Mach number within the studied range;

– the dependencies of the normal force and pitching moment coefficients on the angle of attack approach to linear ones; and

– the variation of the model rolling angle about the longitudinal axis within the range of $\gamma = 0^\circ$–45° actually does not influence the aerodynamic characteristics. The observed differences at different γ lie within the confidential interval of the error.

The pressure and heat fluxes distributions measured on the surface show the presence of the separation region resulting from the interaction between the shock wave generated by the flap and the boundary layer on the body. Increased roughness of the nose part (a layer of powder of about 20 μm) resulted in considerable increasing of the heat-fluxes level on the body, shortening separation region before the flap and thermal load redistribution over the flap surface, the maximum heat flux level on it being decreased. It can be assumed that the surface roughness has changed the flow character in the boundary layer, namely, has caused the laminar flow transition to the turbulent one.

REFERENCES

1. Walpot, L., and H. Ottens. 2002. FESART/EXPERT aerodynamic and aerothermodynamic analysis of the RAV and KHEOPS configuration. Technical Report. TOS-MPA/2718/LW. ESTEC.
2. Ottens, H., and L. Walpot. 2003. EXPERT model 4.2, Model description and trajectory analysis. Technical Report. TOS-MPA/2749/HO. ESTEC.
3. Danilkin, V. 2002. Pre-contractual studies of the possibility to launch re-entry vehicles by Volna LV for aerothermodynamic investigations. Technical Report. 000/113-40-2002. Makeyev Design Bureau.
4. Kharitonov, A. M., V. I. Zvegintsev, M. D. Brodetsky, I. I. Mazhul, J. M. Muylaert, W. Kordulla, and J. C. Paulat. 2005. Aerodynamic investigation of aerospace vehicles in the new hypersonic wind tunnel AT-303 in ITAM. *4th Symposium (International) on Atmospheric Re-Entry Vehicles and Systems*. Arcachon, France.
5. Kharitonov, A. M., N. P. Adamov, M. D. Brodetsky, L. G. Vasenyov, I. I. Mazhul, V. I. Zvegintsev, J. C. Paulat, J. M. Muylaert, and W. Kordulla. 2006. Investigation of aerogasdynamics of re-entry vehicles in the new hypersonic wind tunnel at ITAM. AIAA Paper No. 2006-0499.
6. Kharitonov, A. M., N. P. Adamov, M. D. Brodetsky, L. G. Vasenyov, I. I. Mazhul, and V. I. Zvegintsev. 2006. Investigation of aerogasdynamics of re-entry vehicles in the new hypersonic wind tunnel at ITAM. *6th China–Russia High-Speed Flow Conference Proceedings*. Mianyang Sichuan.

7. Adamov, N. P., M. D. Brodetsky, L. G. Vasenyov, I. I. Mazhul, V. I. Zvegintsev, A. M. Kharitonov, J. C. Paulat, J. M. Muylaert, and W. Kordulla. 2006. Aerodynamics of re-entry vehicles at natural Reynolds numbers. *Thermophys. Aeromechanics* 13(3):341–51.
8. Adamov, N. P., A. M. Kharitonov, I. I. Mazhul, L. G. Vasenyov, V. I. Zapryagaev, V. I. Zvegintsev, and J. M. Muylaert. 2008. Investigations of aerogasdynamics of re-entry ballistic vehicle expert. *14th Conference (International) of Aerophysical Research Proceedings*. Novosibirsk, Russia. CD-ROM. ISBN 978-5-98901-040-0.
9. Shettino, A., R. Votta, P. Roncioni, M. Di Clemente, M. Gerritsma, C. Chiarelli, and D. Ferrarella. 2007. Aerodynamic and aerothermodynamic data base of EXPERT capsule. *West–East High-Speed Flow Field Conference Proceedings*. Moscow, Russia.
10. Kharitonov, A. M., V. I. Zvegintsev, L. G. Vasenyov, A. D. Kuraeva, D. G. Nalivajchenko, A. V. Novikov, M. A. Paikova, V. F. Chirkashenko, N. V. Shakhmatova, and S. I. Shpak. 2006. Characteristics of the AT-303 hypersonic wind tunnel. Part 1. Velocity fields. *Thermophys. Aeromechanics* 13(1):1–16.